

# Long-term reliability of gate oxide in Cascode GaN power devices under proton irradiation with different energies\*

Ru-Xue Bai,<sup>1</sup> Hong-Xia Guo,<sup>2,†</sup> Yang-Fan Li,<sup>1</sup> Wu-Ying Ma,<sup>2</sup> Ji-Fang Li,<sup>1</sup> Feng-Qi Zhang,<sup>2</sup> Xiao-Ping Ouyang,<sup>2</sup> and Xiang-Li Zhong<sup>1,‡</sup>

<sup>1</sup>*The School of Materials Science and Engineering, Xiangtan University, Xiangtan 411105, China*

<sup>2</sup>*Northwest Institute of Nuclear Technology, Xian 710024, China*

In this paper, the effects of proton irradiation with different energies on the long-term reliability of gate-oxide in Cascode enhanced GaN power device are studied. The typical degradation of electrical properties was observed. In contrast, the gate current was increased by about two orders of magnitude after 25 MeV and 60 MeV proton irradiation, while the gate current was unchanged significantly after 100 MeV proton irradiation. By using the time-dependent dielectric breakdown (TDDB) method confirms that the risk of gate current leakage is increased under proton irradiation. The breakdown time of the gate dielectric becomes shorter after proton irradiation, which is not conducive to the long-term and stable application of GaN power devices. In addition, SRIM simulation results based on Monte Carlo indicated that the interaction cross section between low-energy protons and target nuclei is larger, which will cause more defects in the device, leading to the low-energy proton damage becoming more severe. Proton irradiation produces defects in the gate-oxide layer that shorten the breakdown time of the device gate-oxide layer, ultimately resulting in reduced long-term reliability of the device.

Keywords: Proton irradiation, Cascode GaN power devices, Long-term reliability, TDDB, Monte Carlo simulation

## I. INTRODUCTION

With the continuous development of high-power electric propulsion technology for space systems and satellite platforms, the devices with high-frequency, high-power, high-temperature, high-voltage and radiation-resistant have gradually become the development direction of high-efficiency power electronics systems [1–3]. As a typical representative of the third generation of wide-band-gap semiconductors, GaN materials have outstanding characteristics such as wide-band-gap (3.4 eV), high breakdown electric field ( $5 \times 10^6$  V/cm) and strong radiation resistance ( $10^{10}$  rad). This makes GaN-based power devices the most attractive candidates for space power systems [4–10]. Therefore, it is important to study the long-term reliability of GaN-based devices in space radiation environments.

In fact, electronic devices working in aerospace will inevitably be damaged by energetic particles from a complex radiation environments [11–13]. Among them, protons are the most common particles in the space radiation environment, which has the characteristics of high energy and high fluence, and is a threat to aerospace electronic equipment [14–16]. Due to the high bond strength of N-Ga and N-Al in GaN HEMT devices, the resulting compounds such as GaN, AlN, and AlGaN exhibit high stability, which can generate a high displacement damage energy threshold (19~25 eV). Additionally, the two-dimensional electron gas (2DEG) in GaN is insensitive to defects, so GaN power devices have strong resistance to displacement damage. GaN has a wide bandgap and theoretically exhibits excellent resistance to ionizing ra-

diation. However, in practice, GaN materials contain a high density of defects, and current GaN devices have high process requirements. These factors pose significant challenges to the radiation resistance characteristics of GaN power devices. Previous studies have shown that GaN-based devices are at risk of degradation or failure when exposed to radiation environments [17–25].

Therefore, the effect of proton irradiation on GaN-based power devices cannot be ignored. Numerous proton irradiation experiments have been performed for GaN-based power devices [26–31]. Yue et al. [30], performed 3 MeV proton irradiation experiment on AlGaN/GaN HEMT with a total fluence reaching  $5 \times 10^{14}$  p/cm<sup>2</sup>. The results show that the saturation current of the device is reduced by 14.6%, the threshold voltage ( $V_{th}$ ) is shifted forward by 0.35 V and the inverse gate current is significantly reduced. The main degradation mechanism is thought to be an increase in the density of the negatively charged trap in the channel. Kim et al. [31], carried out proton irradiation experiments at 0.5 MeV, 5 MeV and 60 MeV in AlGaN/GaN HEMT. The results show that the transfer properties decay the most after 0.5 MeV irradiation because the low proton energy produces a larger loss of non-ionizing energy. The gate leakage current of the fabricated HEMTs decreased by increasing the irradiation energy is due to the formation of an interfacial oxide layer caused by proton radiation between the gate and AlGaN layer. However, although these reports describe the mechanisms of degradation of the electrical performance of GaN devices, they do not indicate the impact of these degradations on the lifespan of device. It is important to note that the most critical characteristic of aerospace components is long-term reliability. Therefore, further research is needed to achieve the long-term stable space application of GaN power devices.

In this work, the long-term reliability of the gate oxide of Cascode GaN power devices is investigated for different energies of proton radiation. Using the time-dependent dielectric

\* This work was supported by the National Natural Science Foundation of China (Nos. 12275230 and 12027813)

† Corresponding author, guohxnint@126.com

‡ Corresponding author, xlzhong@xtu.edu.cn

66 breakdown (TDDB) method, it was found that the time toler-  
 67 ance for gate oxide breakdown of the device after low-energy  
 68 proton irradiation is the shortest. Furthermore, the SRIM sim-  
 69 ulation method was employed to elucidate the basic mech-  
 70 aism of the enhanced damage effect owing to low-energy pro-  
 71 ton irradiation.

## 72 II. SAMPLE AND METHODS

### 73 A. Sample

74 The samples selected for this experiment are Common  
 75 gate and Common source (Cascode) structure enhanced GaN  
 76 power devices from Transphorm. The device consists of a  
 77 high voltage depletion GaN HEMT and a low voltage en-  
 78 hanced Si MOSFET, and the device structure is shown in  
 79 Fig. 1 (a). Since the drain source voltage of the Si MOSFET  
 80 provides a negative bias voltage to the gate-source voltage  
 81 of GaN HEMT, the on-off of GaN HEMT can be controlled  
 82 by controlling the on-off of Si MOSFET, thus achieving the  
 83 normally closed characteristic. Fig. 1 (b) shows the device  
 84 package diagram. We used FIB and SEM methods to analyze  
 85 the layered structure of Cascode GaN power devices, and the  
 86 results are shown in Fig. 1(c). The operating voltage rated for  
 87 GaN power devices is 650 V, and the threshold voltage is 3.3  
 88 V to 4.8 V.

### 89 B. Irradiation experiments

90 The proton experiment was carried out on Xi'an 200 MeV  
 91 Proton Accelerator Facility (XiPAF). Protons with energies of  
 92 25 MeV, 60 MeV and 100 MeV were used for experiments.  
 93 The total fluence during the experiment was set to  $2 \times 10^{11}$   
 94 and  $5 \times 10^{11} \text{ p/cm}^2$ , and the fluence rate was about  $2 \times 10^9$   
 95  $\text{p/cm}^2 \cdot \text{s}$ . The irradiation time is about 100 s to 250 s. The  
 96 bias voltages of 550 V, 600 V and 650 V were applied to  
 97 the sample, respectively. The experimental temperature was  
 98 room temperature. Irradiate two to three samples under each  
 99 experimental condition to eliminate randomness.

### 100 C. Time-dependent dielectric breakdown methods (TDDB)

101 Since the 1990s, TDDB testing has been widely used for  
 102 the quality assessment of gate oxide in power MOSFETs [32].  
 103 According to the method of applying the electric field to the  
 104 device, TDDB lifetime prediction can be divided into con-  
 105 stant voltage (current) and ramp voltage (current). In this arti-  
 106 cle, we use the constant voltage method, which can obtain the  
 107 failure time of the device, evaluate the quality of gate oxide of  
 108 the device through Weibull distribution statistics, and further  
 109 estimate the lifespan of the gate oxide layer. The constant  
 110 voltage TDDB test is conducted at a voltage slightly lower  
 111 than the gate breakdown voltage to determine the breakdown  
 112 time and analyze the results. The slightly lower voltage it-  
 113 self is not sufficient to cause intrinsic breakdown. However,

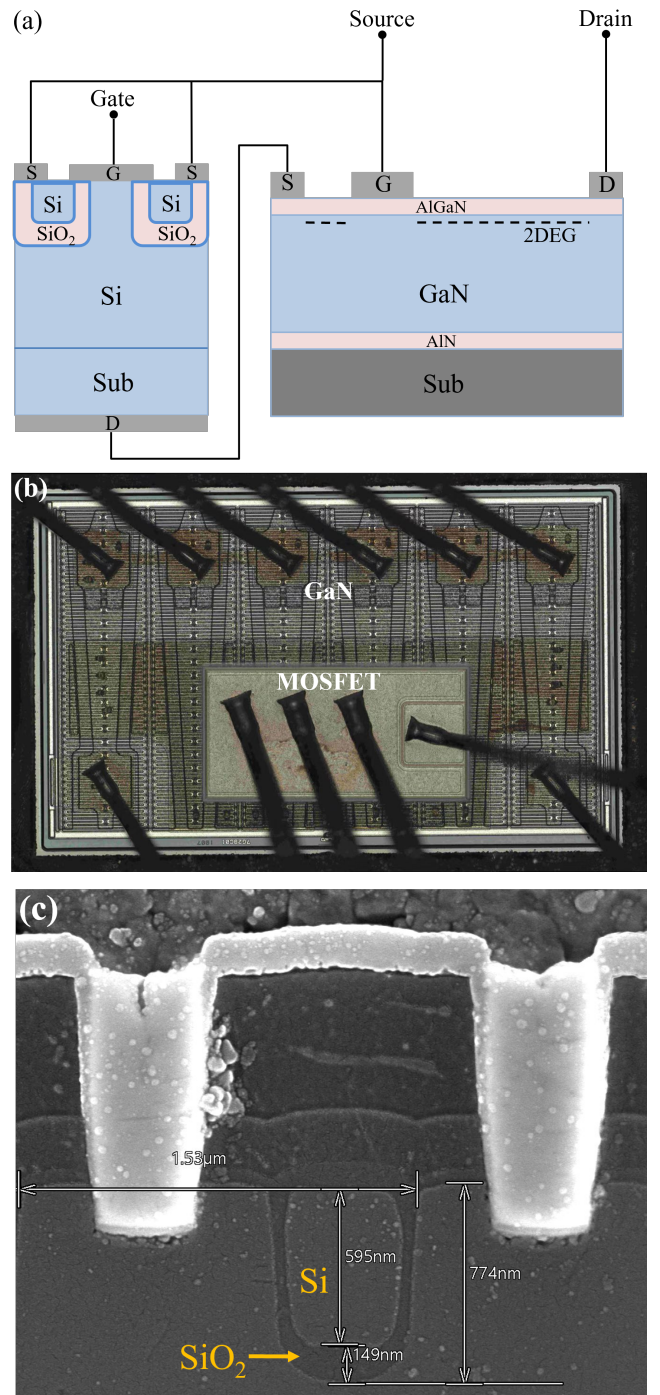


Fig. 1. **a** The structure diagram, **b** the package diagram, and **c** the SEM image of Cascode GaN power device.

114 because of defects in the oxide layer during the application  
 115 of electrical stress, after a certain period, charges accumu-  
 116 late near the defects or are captured by the defects, leading to  
 117 breakdown. Time-dependent gate oxide breakdown is a ma-  
 118 jor factor affecting device reliability. Generally speaking, the  
 119 breakdown occurs due to a high electric field and excessive  
 120 current in the oxide layer, leading to charge accumulation.

121 **D. Stopping and Range of Ions in Matter simulation method  
122 (SRIM)**

123 SRIM uses the Monte Carlo method to track the motion of  
124 a large number of incident particles through computer simula-  
125 tion [33]. It is possible to calculate various physical processes  
126 of particle beams in different materials, including scattering,  
127 escape, energy deposition, transport, and the analysis of the  
128 radiation hardening characteristics of materials. The position  
129 of the particle, the energy loss, and various secondary par-  
130 ticles parameters are stored throughout the tracking process.  
131 The collision parameters are randomly selected to simulate  
132 the collision process and calculate the process of incident ions  
133 colliding from the moment they enter the target until they lose  
134 energy and stop or exit the target. Finally, obtain the expected  
135 values of various required physical quantities and the corre-  
136 sponding statistical errors. Since the results of the calcula-  
137 tions have statistical significance, only when the number of  
138 ions calculated is sufficiently large can the required calcu-  
139 lation accuracy be achieved. SRIM provides two different  
140 interfaces: as shown in Figure 2 (a), the SRAM program in-  
141 terface allows users to input the state of the target material  
142 and the incident particles and set the energy range of the in-  
143 cident particles. This interface is mainly used to calculate  
144 the penetration depth of particles with different energies in  
145 the target material. The other interface is the TRIM program  
146 interface, as shown in Figure 2 (b). Through this interface,  
147 users can calculate parameters related to the energy loss of  
148 particle beams in target materials, the number of vacancies  
149 produced, and the slowing of radiation damage to materials.  
150 In this article, the functionality of TRIM is mainly used.

151

### III. RESULTS AND DISCUSSION

152

#### A. I-V characteristic results

153 The (I-V) characteristic curves of Cascode structure en-  
154 hanced GaN power devices before and after proton irradiation  
155 are shown in Fig. 3. The device threshold voltage changes  
156 after proton irradiation with energies of 25 MeV, 60 MeV  
157 and 100 MeV are given in Fig. 3 (a). As can be seen in  
158 the figure, the threshold voltage of the devices shown neg-  
159 atively drifted after proton irradiation. Data are statistically  
160 presented in Table 1. The threshold voltage drift becomes  
161 more pronounced with an increase in proton fluence and bias  
162 voltage, which is consistent with previous experimental re-  
163 sults [34–36]. The gate characteristics of the devices are rep-  
164 resented by Fig. 3(b), from which it can be seen that the  
165 gate damage of the devices with 25 MeV and 60 MeV pro-  
166 tons irradiation is more severe. After 25 MeV irradiation,  
167 the gate leakage current increases from  $4.18 \times 10^{-12}$  A to  
168  $4.42 \times 10^{-10}$  A. After 60 MeV irradiation, the gate leakage  
169 current increased from  $3.88 \times 10^{-12}$  A to  $3.81 \times 10^{-10}$  A. The  
170 gate leakage current increases by two orders of magnitude.  
171 The gate characteristics of the devices are almost unchanged  
172 after 100 MeV proton irradiation. Fig. 3(c) shows the out-  
173 put characteristic curves of the device, which shows a slight

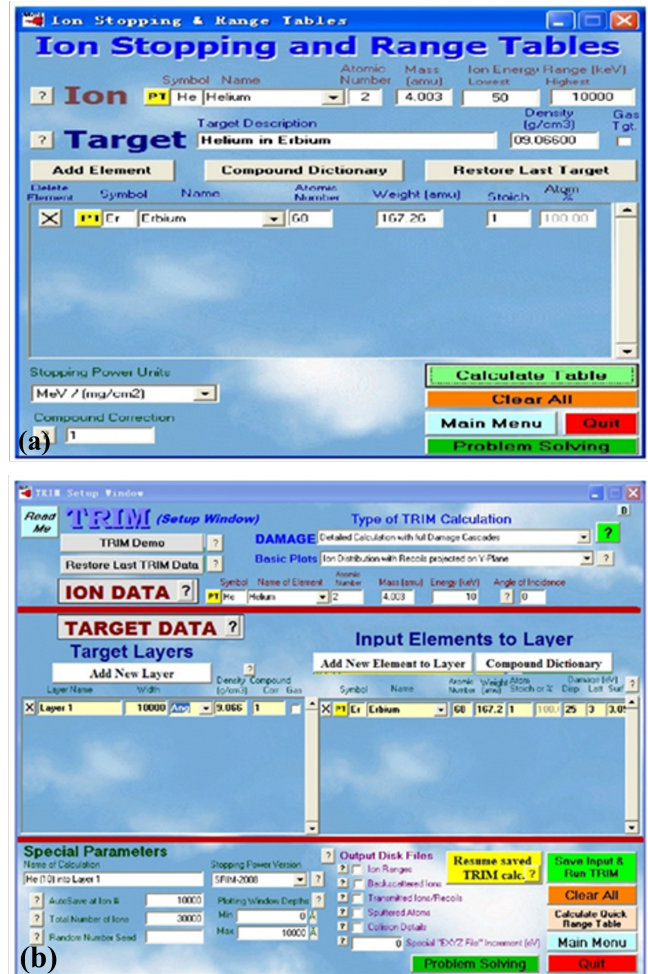


Fig. 2. **a** SRAM program interface and **b** TRIM program interface

Table 1. The threshold voltage of Cascode GaN power device under various proton energies and bias voltages.

Energy	Bias	$V_{th}$	$V_{th}(V)_{radiation}$	
		$(V)_{non-radiation}$	$2 \times 10^{11} p/cm^2$	$5 \times 10^{11} p/cm^2$
25 MeV	550 V		2.8	1.7
	600 V	3.4	2.6	1.7
	650 V		2.3	1
60 MeV	550 V		2.8	1.9
	600 V	3.4	2.8	1.8
	650 V		2.5	1.3
100 MeV	550 V		2.9	2.1
	600 V	3.4	2.8	1.9
	650 V		2.6	1.6

174 increase in the drain leakage current after protons irradiation.

175 By comparison of the changes in the electrical character-  
176 istics of the devices before and after proton irradiation, it is  
177 found that these degradations are mainly caused by gate dam-  
178 age. This manifests itself as a negative drift of threshold volt-  
179 age and an increase in gate leakage current. The threshold  
180 voltage negative drift indicates that the switching capability  
181 of the gate is degraded. The gate characteristics of the Cas-  
182 code GaN power device are mainly controlled by the Si MOS-

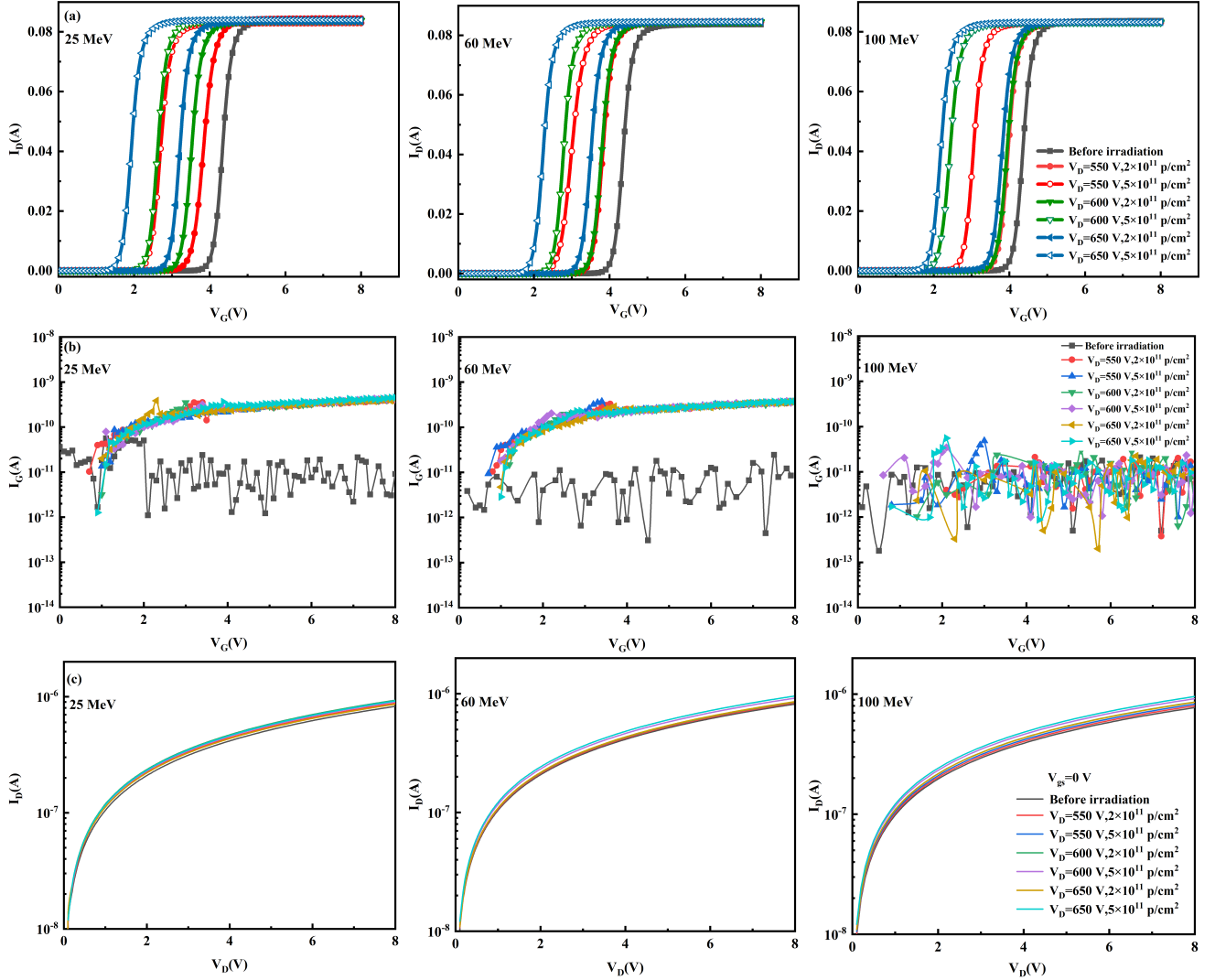


Fig. 3. Electrical characterization diagram of Cascode GaN power device **a**  $I_D$ - $V_G$ , **b**  $I_G$ - $V_G$ , and **c**  $I_D$ - $V_D$ .

183 FETs, as can be seen from the presentation in Fig. 1(a). For  
 184 gate oxide transistors, the threshold voltage drift is due to a  
 185 combination of oxide trap charge and interface trap charge  
 186 [37]:

$$187 \Delta V_{th} = \Delta V_{ot} + \Delta V_{it},$$

199 oxide trap charge generated by proton irradiation plays a ma-  
 200 jor role in the threshold voltage drift. The increase of gate  
 201 leakage current indicates the deterioration of insulation char-  
 202 acteristics of gate. The degradation of the insulating proper-  
 203 ties of the gate oxide is usually caused by defects or conduc-  
 204 tive channels generated by localized hot carrier stresses in the  
 205 drain [38]. From the above analysis, it can be concluded that  
 206 the defects generated in the oxide layer are the main reason  
 207 for the degradation of the device gate characteristics due to  
 208 proton irradiation.

190 where  $\Delta V_{ot}$  is the oxide trap charge,  $\Delta V_{it}$  is the interface trap  
 191 charge,  $C_{OX}$  is the capacitance per unit area of the gate ox-  
 192 ide layer,  $t_{ox}$  is the oxide layer thickness, and  $\rho_{ot,it}(x)$  is the  
 193 charge distribution of the radiation-induced oxide trap charge  
 194 or interface trap charge. At high dose rates and short periods  
 195 of time, the neutralization of the oxide trap charge is small,  
 196 resulting in a high oxide trap charge density. In contrast, in-  
 197 terfacial trap charges do not have enough time to accumulate  
 198 and usually have small densities [37]. In other words, the

209  
 210 In order to reveal the effect of proton irradiation introduc-  
 211 ing defects in the gate oxide layer on the long-term reliability  
 212 of the gate oxide layer of Cascode GaN power device, we will  
 213 compare the breakdown time of gate dielectric before and af-  
 214 ter irradiation using the TDDDB experimental method. TDDDB

## B. TDDDB test results and discussion

experiment adopts the constant voltage stress (CVS) method. First, the time-zero dielectric breakdown (TZDB) method is used to determine the accelerated stress test range. It is specified that the breakdown occurs when the gate current reaches 0.1 A.

As shown in Fig. 4(a), when the gate voltage reaches about 47 V, the device will be broken down instantly. In order to complete the experiment more accurately and quickly, the bias voltage  $V_{GS}=45$  V is selected in the TDDB test. Fig. 4(b) shows the curve of the gate leakage current of the devices before and after proton irradiation as a function of time under constant stress at the gate. As can be seen from the figure, the device gate leakage current continues to decrease before breakdown. This is the gate breakdown characteristic of silicon-based devices, which further indicates that the gate damage caused by proton irradiation is dominated by the damage of cascading Si-based transistors. The decrease in current indicates that the net negative charge in the device is captured [39]. The breakdown time of the unirradiated devices is about 28225 s. After 100 MeV proton irradiation of the device, the breakdown time is almost constant, about 27985 s. The breakdown time of the device after 60 MeV proton irradiation is about 26892 s, which is shortened by about 4.72%. The breakdown time of the device after 25 MeV proton irradiation is about 22535 s, which is shortened by about 20.16%.

The TDDB failure models widely used at present include E model and 1/E model [40, 41]. The E model also known as the thermochemical model, is suitable for devices with thicker gate oxide layers. The 1/E model is more suitable for devices with gate oxide layer thickness <5 nm. As shown in Fig. 1(c), the thickness of the gate oxide layer of the experimental sample is about 149 nm, so the E model should be used for failure analysis. The basic idea of the E model is that as the defects in the oxide layer increase, when the defects in the oxide layer are connected into a leakage path, the oxide layer will break down. Fig. 5 shows a schematic diagram of the leakage paths in the oxide layer before and after proton irradiation. When a high voltage is applied between the upper and lower interfaces of the oxide layer, the defects in the oxide layer will form electron traps, randomly distributed within the oxide layer. Each electron trap has the ability to capture electrons under influence of the electric field in the oxide layer. After proton irradiation, the number of defects in the oxide layer increases, and the regions where electron traps capture electrons may overlap, forming a current path from the upper interface of the oxide layer to the lower interface, as shown in Fig. 5(b). Therefore, proton irradiation leads to a reduction in the gate-oxide layer breakdown time of the device.

It is also common to utilize the gate oxide layer cumulative charge to assess the magnitude of the device breakdown time, and thus the gate oxygen layer lifetime. The cumulative charge is shown by eq. (3) [38]:

$$Q_{BD} = \int_0^{t_{BD}} J dt \quad (3)$$

Where  $t_{BD}$  is the gate-oxide breakdown time;  $J$  is the gate

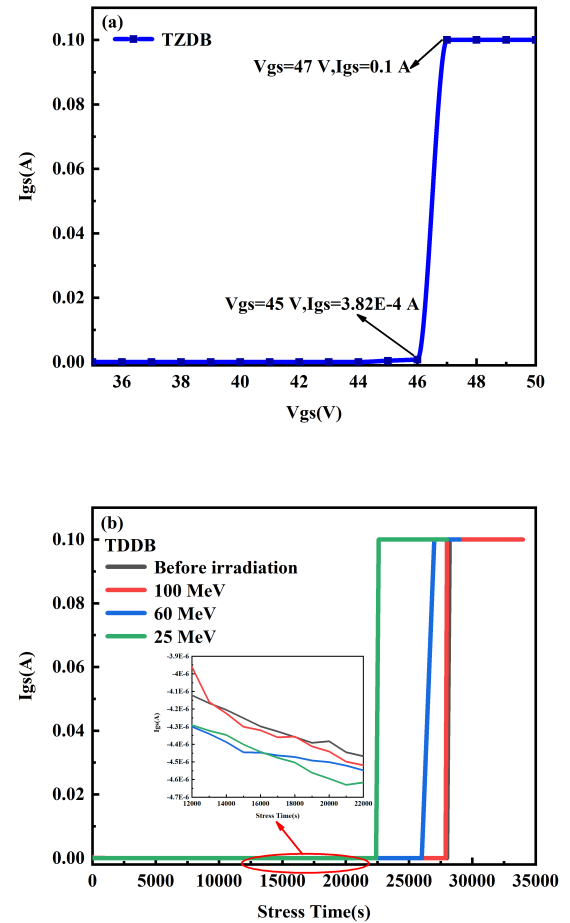


Fig. 4. **a** Time-zero dielectric breakdown test curve, **b** time-dependent dielectric breakdown test curve.

leakage current. According to the calculation,  $Q_{BD}$  is 0.197 C before proton irradiation,  $Q_{BD}$  is 0.212 C after 100 MeV proton irradiation,  $Q_{BD}$  is 0.275 C after 60 MeV proton irradiation, and  $Q_{BD}$  is 0.299 C after 25 MeV proton irradiation, which increases by 40% compared with before irradiation. The accumulated charge of the gate oxide layer increases after irradiation and the lifetime of the gate oxide layer decreases. This charge-to-breakdown value has been used for several years as the most important reliability figure-of-merit for oxides.

### C. SRIM simulation results and discussion

Through the analysis of proton irradiation experiment and TDDB experiment results, it is found that the influence of 100 MeV proton irradiation on the device is smaller than 25 MeV and 60 MeV, and the phenomenon of low energy damage is more serious. This is due to the fact that protons travel essentially in a straight line through the material. The higher proton energy, the smaller interaction cross section between

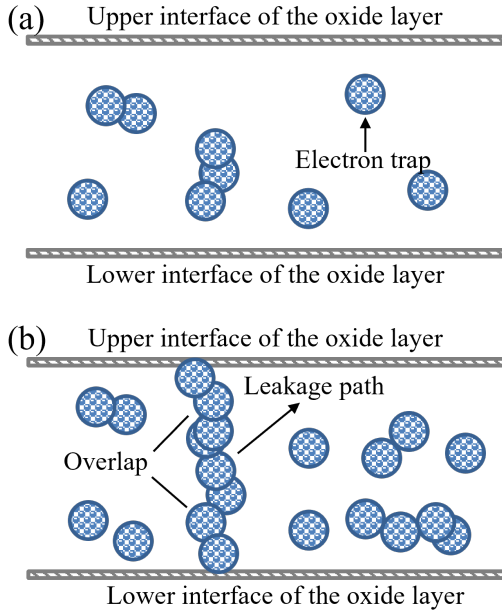


Fig. 5. Schematic diagram of the leakage paths in the oxide layer **a** before and **b** after proton irradiation.

the proton and the target nucleus, and the smaller average energy transferred to the target nucleus [42, 43]. With the increase of proton energy, the radiation damage region gradually moves deeper into the device, away from the sensitive gate oxide layer region. We simulated the interaction cross sections between proton at different energies and target using SRIM software, as shown in Fig. 6. The simulation results confirm the above statement that the irradiation damage region gradually moves away from the gate oxide layer as the proton energy increases (marked by the red arrow). The interaction radii of protons at 25 MeV, 60 MeV, and 100 MeV are  $6 \times 10^{-8}$ ,  $2.8 \times 10^{-8}$  and  $2 \times 10^{-8}$  Ang/Ion, respectively. In comparison, the cross-sectional radius produced by 25 MeV proton irradiation (circled in red dashed lines) is the largest. We also simulated the number of vacancies generated by protons of different energies in Si MOSFET transistors, as shown in Fig. 6(d). Among them, the 25 MeV protons produce the most vacancy defects in the device's sensitive layer. These two factors eventually lead to enhanced damage of low-energy proton irradiation. The simulation results are consistent with the experimental analysis results. The simulation results and the experimental analysis results have mutually verified each other.

#### IV. CONCLUSION

In summary, the impact of proton irradiation at different energies on the long-term reliability of the gate oxide in the Cascode GaN power devices has been investigated. Through the analysis of experimental results combined with the device electrical characteristics formula, the oxide trap charges in-

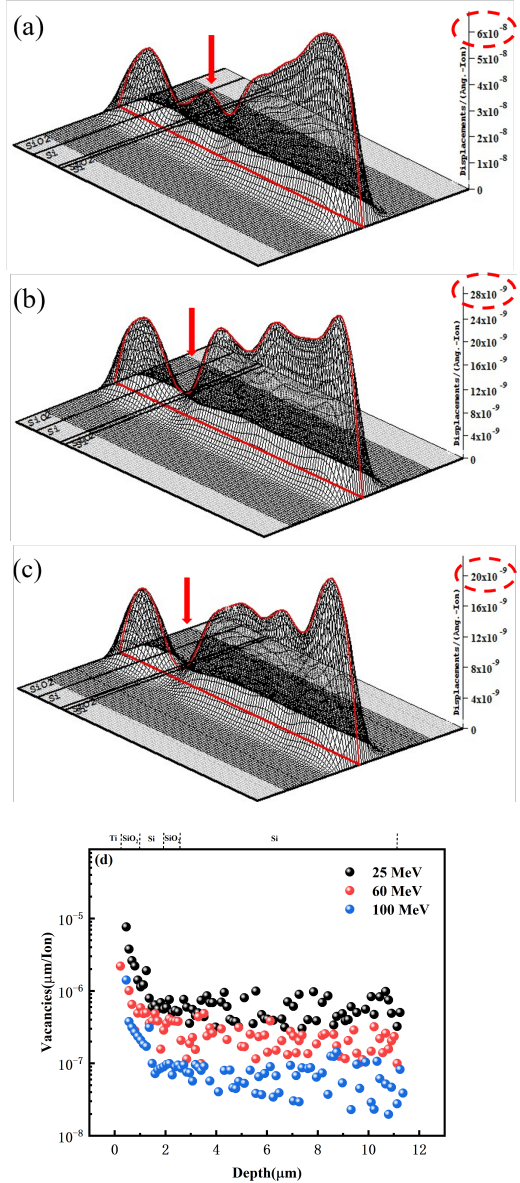


Fig. 6. Trajectory diagram of proton incident Cascode GaN power device **a** 25 MeV **b** 60 MeV **c** 100 MeV and **d** the vacancy.

troduced by proton irradiation in the oxide layer are the main factors leading to the deterioration of the device's gate performance. The degradation of gate performance indicates that gate switching capability and gate insulation characteristics are damaged, which is detrimental to the long-term reliable application of the device. To this end, we used the TDDB experimental method to test the gate tolerance of the device before and after proton irradiation. We applied a constant gate bias voltage of  $V_{GS}=45$  V to both the unirradiated and irradiated devices. The experimental results show that the gate dielectric breakdown time of the irradiated device becomes shorter and the lifetime of the gate oxide layer of the device decreases. This is because proton irradiation introduces defects in the device's oxide layer, which form electron

traps that capture electrons under the influence of an electric field. The accumulation of a large number of electron traps will form one or more channels from the upper interface of the oxide layer to the lower interface, which serve as leakage paths. When the traps capture enough electrons, the device gate will undergo breakdown. Furthermore, it has been found that 25 MeV and 60 MeV protons cause more damage to the device than 100 MeV protons. We used the SRIM method to simulate the interaction between protons of different energies and the device, which well explained this phenomenon. The simulation results indicate that 25 MeV proton irradiation introduces more vacancy defects into the device. The radiation damage area of low-energy protons is closer to the device's

sensitive area and has a larger effective range. The results of this paper can provide theoretical support for further improving the long-term reliability of gate oxide in Cascode GaN power devices.

**Author contributions** All authors contributed to the study conception and design. Material preparation, data collection and analysis were performed by Ru-Xue Bai, Hong-Xia Guo, Yang-Fang Li, Wu-Ying Ma and Ji-Fang Li. The first draft of the manuscript was written by Ru-Xue Bai and all authors commented on previous versions of the manuscript. All authors read and approved the final manuscript.

**Data availability** The data that support the findings of this study are openly available in Science Data Bank.

- 
- [1] B. Mounika, J. Ajayan, S. Bhattacharya, et al., Recent developments in materials, architectures and processing of AlGaN-/GaN HEMTs for future RF and power electronic applications: A critical review. *Micro and Nanostructures*. **168**, 207317 (2022). <https://doi.org/10.1016/j.sse.2022.108571>
- [2] Y. Yuan, S. Q. Zhou, X. Q. Wang, Modulating properties by light ion irradiation: From novel functional materials to semiconductor power devices. *Journal of Semiconductors*. **43**, 063101 (2022). <https://doi.org/10.1088/1674-4926/43/6/063101>
- [3] Y. Tang, L. Wang, X. W. Cai, et al., Investigation on performance degradation mechanism of GaN p-i-n diode under proton irradiation. *Appl. Phys. Lett* **122**, 022101 (2023). <https://doi.org/10.1063/5.0130017>
- [4] N. R. Glavin, K. D. Chabak, E. R. Heller, et al., Flexible gallium nitride for high-performance, strainable radio-frequency devices. *Adv. Mater* **29**, 1701838 (2017). <https://doi.org/10.1002/adma.201701838>
- [5] X. Li, P. E. Wang, X. Zhao, et al., Defect and impurity-center activation and passivation in irradiated AlGaN/GaN HEMTs. *IEEE Trans. Nucl. Sci.* **71**, 80-87 (2024). <https://doi.org/10.1109/TNS.2023.3336836>
- [6] W. J. Yan, Y. Y. Xue, W. J. Zhou, et al., Au ion irradiation induces ultralow thermal conductivity in GaN. *Appl. Phys. Lett* **125**, 032202 (2024). <https://doi.org/10.1063/5.0220863>
- [7] D. M. Fleetwood, E. X. Zhang, R. D. Schrimpf, et al., Radiation effects in AlGaN/GaN HEMTs. *IEEE Trans. Nucl. Sci.* **69**, 1105-1119 (2022). <https://doi.org/10.1109/TNS.2022.3147143>
- [8] S. J. Pearton, R. Deist, F. Ren, et al., Review of radiation damage in GaN-based materials and devices. *J. Vac. Sci. Technol. A* **31**, 050801 (2013). <https://doi.org/10.1116/1.4799504>
- [9] T.P. Chow, R. Tyagi, Wide bandgap compound semiconductors for superior high-voltage unipolar power devices. *IEEE Trans. Electron Dev. Sci.* **41**, 1481-1483 (1994). <https://doi.org/10.1109/ISPSD.1993.297113>
- [10] W. Saito, Y. Takada, M. Kuraguchi et al., High breakdown voltage AlGaN/GaN power-HEMT design and high current density switching behavior. *IEEE Trans. Electron Dev. Sci.* **50**, 2528-2531 (2003). <https://doi.org/10.1109/TED.2003.819248>
- [11] J.M. Osheroff, J. M. Lauenstein, R. L. Ladbury, LET and range characteristics of proton recoil ions in gallium nitride (GaN). *IEEE Trans. Nucl. Sci.* **68**, 597-602 (2021). <https://doi.org/10.1109/TNS.2021.3050980>
- [12] F. Mirkhosravi, A. Rashidi, A. T. Elshafiey, et al., Effects of fast and thermal neutron irradiation on Ga-polar and N-polar GaN diodes. *J. Appl. Phys.* **133**, 015704 (2023). <https://doi.org/10.1063/5.0119294>
- [13] W. Tang, H. Li, M. Xu, et al., Neutron irradiation influence on high-power thyristor device under fusion environment. *Nucl. Sci. Tech.* **35**, 72 (2024). <https://doi.org/10.1007/s41365-024-01433-1>
- [14] R. Eccoett, Overview of in-orbit radiation induced spacecraft anomalies. *IEEE Trans. Nucl. Sci.* **60**, 1791-1815 (2013). <https://doi.org/10.1109/TNS.2013.2262002>
- [15] J. Chen, Z. Q. Feng, J. S. Wang, Nuclear in-medium effects on  $\eta$  dynamics in proton-nucleus collisions. *Nucl. Sci. Tech.* **27**, 73 (2016). <https://doi.org/10.1007/s41365-016-0069-7>
- [16] H. Zhang, H. X. Guo, F. Q. Zhang, et al., Study on proton-induced single event effect of SiC diode and MOSFET. *Microelectron. Reliab.* **124**, 114329(2021). <https://doi.org/10.1016/j.microrel.2021.114329>
- [17] L. Lv, J. G. Ma, Y. R. Cao, et al., Study of proton irradiation effects on AlGaN/GaN high electron mobility transistors. *Microelectron. Reliab.* **51**, 2168-2172 (2011). <https://doi.org/10.1016/j.microrel.2011.04.022>
- [18] S.J. Pearton, F. Ren, E. Patrick et al., Review-Ionizing radiation damage effects on GaN devices. *ECS J. Solid State Sci. Technol* **5**, Q35-Q60 (2016). <https://doi.org/10.1149/2.0251602jss>
- [19] F. Zhou, C. Zan, T. Y. Zhou, et al., Irradiation hardened p-GaN HEMTs enabling 558 V single-event hardness at 75.7 MeV $\mu$ cm<sup>2</sup>/mg and 95% conversion efficiency at 300 W/500 kHz. *IEEE Electron Dev Lett.* **45**, 976-979 (2024). <https://doi.org/10.1109/LED.2024.3386799>
- [20] A.Y. Polyakov, S.J. Pearton, P. Frenzer et al., Radiation effects in GaN materials and devices. *J. Mater. Chem. C. Sci.* **5**, 877-887 (2013). <https://doi.org/10.1039/C2TC00039C>
- [21] L.Q. Zhang, C.H. Zhang, C.L. Xu et al., Damage produced on GaN surface by highly charged Krq+ irradiation. *Nucl. Sci. Tech.* **28**, 176 (2017). <https://doi.org/10.1007/s41365-017-0326-4>
- [22] C. H. Sun, C. Peng, Z. G. Zhang, et al., Mechanism of reverse gate leakage current reduction in AlGaN/GaN high-electron-mobility-transistor after 3-MeV proton irradiation. *Appl. Phys. Lett.* **121**, 072109 (2022). <https://doi.org/10.1063/5.0102366>
- [23] Y. Li, S. T. Jiang, H. Y. He, et al., Radiation-induced defects in the InGaN/GaN superlattice structure. *Phys. Scr.* **99**, 065407 (2024). <https://doi.org/10.1088/1402-4896/ad4794>
- [24] G.P. Liu, X. Wang, M.N. Li et al., Effects of high-energy proton irradiation on separate absorption and multiplication GaN avalanche photodiode. *Nucl. Sci. Tech.* **29**, 139 (2018).

- 449 <https://doi.org/10.1007/s41365-018-0480-3>

450 [25] P. P. Hu, L. J. Xu, S. X. Zhang, et al., Failure mechanisms  
451 of AlGaN/GaN HEMTs irradiated by highenergy heavy ions  
452 with and without bias. Nucl. Sci. Tech. **36**, 13 (2025). <https://doi.org/10.1007/s41365-024-01567-2>

453 [26] Z. Zhang, A. R. Arehart, E. Cinkilic, et al., Impact of proton  
454 irradiation on deep level states in n-GaN. Appl. Phys. Lett. **103**,  
455 042102 (2013). <https://doi.org/10.1063/1.4816423>

456 [27] X. Wan, O. K. Baker, M. W. McCurdy, et al., Low energy  
457 proton irradiation effects on commercial enhancement mode  
458 GaN HEMTs. IEEE Trans. Nucl. Sci. **64**, 253-257 (2017).  
459 <https://doi.org/10.1109/TNS.2016.2621065>

460 [28] A. Stockman, A. Tajalli, M. Meneghini, et al., The effect of  
461 proton irradiation in suppressing current collapse in AlGaN/  
462 GaN high-electron-mobility transistors. IEEE Trans. Electron  
463 Dev. Sci. **66**, 372-377 (2019). <https://doi.org/10.1109/TED.2018.2881325>

464 [29] T. Zhu, X. F. Zheng, T. X. Yin, et al., A thorough study on the  
465 electrical performance change and trap evolution of AlGaN/  
466 GaN MIS-HEMTs under proton irradiation. Appl. Phys. Lett.  
467 **122**, 183502 (2023). [vhttps://doi.org/10.1063/5.0146638](https://doi.org/10.1063/5.0146638)

468 [30] S. Z. Yue, Z. F. Lei, C. Peng, et al., High-fluence proton-  
469 induced degradation on AlGaN/GaN high-electron-mobility  
470 transistors. IEEE Trans. Nucl. Sci. **67**, 1339-1344 (2020). <https://doi.org/10.1109/TNS.2020.2974916>

471 [31] D. S. Kim, J. H. Lee, J. G. Kim, et al., Anomalous DC char-  
472 acteristics of AlGaN/GaN HEMTs depending on proton irra-  
473 diation energies. ECS J. Solid State Sci. Technol. **9**, 065005  
474 (2020). <https://doi.org/10.1149/2162-8777/aba32e>

475 [32] M. M. Mathur, J. A. Cooper, Time-dependent-dielectric-  
476 breakdown measurements of thermal oxides on n-type 6H-  
477 SiC. IEEE Trans. Electron Dev. Sci. **46**, 520-524 (1999). <https://doi.org/10.1109/16.748871>

478 [33] J. F. Ziegler, M. D. Ziegler, J. P. Biersack, SRIM - The stopping  
479 and range of ions in matter. Nucl. Instrum. Methods, B. **268**,  
480 1818-1823 (2010). <https://doi.org/10.1016/j.nimb.2010.02.091>

481 [34] Y. X. Lu, R. X. Cao, H. X. Li, et al., Degradation of electrical  
482 performance and radiation damage mechanism of cascode GaN  
483  
484  
485  
486  
487 [35] X. W. Hu, A. P. Karmarkar, B. Jun, et al., Proton-irradiation  
488 effects on AlGaN/AlN/GaN high electron mobility transistors.  
489 IEEE Trans. Nucl. Sci. **50**, 1791-1796 (2003). <https://doi.org/10.1109/TNS.2003.820792>

490 [36] R. D. Harris, L. Scheick, J. P. Hoffman, et al., Radiation  
491 Characterization of Commercial GaN Devices. IEEE Radia-  
492 tion Effects Data Workshop, Las Vegas, NV, USA, 1-5 (2011).  
493 <https://doi.org/10.1109/REDW.2010.6062526>

494 [37] J. R. Schwank, M. R. Shaneyfelt, D. M. Fleetwood, et al., Radia-  
495 tion effects in MOS oxides. IEEE Trans. Nucl. Sci. **55**, 1833-  
496 1853 (2008). <https://doi.org/10.1109/TNS.2008.2001040>

497 [38] G. Groeseneken, R. Degraeve, T. Nigam, et al., Hot carrier  
498 degradation and time-dependent dielectric breakdown in ox-  
499 ides. Microelectronic Engineering **49**, 27-40 (1999). [https://doi.org/10.1016/S0167-9317\(99\)00427-X](https://doi.org/10.1016/S0167-9317(99)00427-X)

500 [39] P. Hazdra, P. Smrkovsky, J. Vobecky et al., Radiation resis-  
501 tance of high-voltage silicon and 4H-SiC power pin diodes.  
502 IEEE Trans. Electron Dev. Sci. **68**, 202-207 (2020). <https://doi.org/10.1109/TED.2020.3038713>

503 [40] J. W. McPherson, H. C. Mogul, Underlying physics of the ther-  
504 mochemical E model in describing low-field time-dependent  
505 dielectric breakdown in SiO<sub>2</sub> thin films. J. Appl. Phys. **84**,  
506 1513-1523 (1998). <https://doi.org/10.1063/1.368217>

507 [41] J. W. McPherson, V. K. Reddy, H. C. Mogul, Field-enhanced  
508 Si-Si bond-breakage mechanism for time-dependent dielectric  
509 breakdown in thin-film SiO<sub>2</sub> dielectrics. J. Appl. Phys. **71**,  
510 1101-1103(1997). <https://doi.org/10.1063/1.119739>

511 [42] I. Jun, M. A. Xapsos, S. R. Messenger, et al., Proton nonioniz-  
512 ing energy loss (NIEL) for device applications. IEEE Trans.  
513 Nucl. Sci. **50**, 1924-1928 (2003). <https://doi.org/10.1109/TNS.2003.820760>

514 [43] S. R. Messenger, E. A. Burke, G. P. Summers, et al., Nonioniz-  
515 ing energy loss (NIEL) for heavy ions. IEEE Trans. Nucl. Sci.  
516 **46**, 1595-1602 (1999). <https://doi.org/10.1109/23.819126>